



Dust-planetary boundary layer interactions amplified by entrainment and advections

Xiaoyan Zhang^{a,b}, Xiyan Xu^c, Haishan Chen^{a,*}, Xiao-Ming Hu^{d,e}, Lan Gao^e

^a Key Laboratory of Meteorological Disaster, Ministry of Education (KLME)/Joint International Research Laboratory of Climate and Environment Change (ILCEC)/ Collaborative Innovation Center on Forecast and Evaluation of Meteorological Disasters (CIC-FEMD), and School of Atmospheric Sciences, Nanjing University of Information Science and Technology, Nanjing, China

^b Department of Occupational and Environmental Health, University of Oklahoma Health Sciences Center, University of Oklahoma, Oklahoma City, OK, USA

^c Key Laboratory of Regional Climate-Environment for Temperate East Asia, Institute of Atmospheric Physics, Chinese Academy of Sciences, Beijing, China

^d Center for Analysis and Prediction of Storms, University of Oklahoma, Norman, OK, USA

^e School of Meteorology, University of Oklahoma, Norman, OK, USA

ARTICLE INFO

Keywords:

Dust aerosols
Planetary boundary layer
Aerosol vertical distribution
Entrainment processes
Nocturnal warm advection

ABSTRACT

Mineral dust contributes to more than half of the global aerosol loading. However, the radiative impacts of dust aerosols on planetary boundary layer (PBL) structure have not been explored sufficiently. During a typical dust storm event over Tarim Basin, dust aerosols exhibit a well-mixed distribution during the daytime in spite of a shallow layer of dust particles accumulated at higher altitudes. By contrast, nocturnal dust plumes are located near the surface due to stable stratification. We demonstrate that these differentiated vertical distributions determine the spatial heterogeneity of dust loading, radiative fluxes and PBL height variations. Dust aerosols cause daytime PBL suppression and nighttime PBL promotion through modulating surface and atmospheric radiative budgets. Specifically, dust-induced cooling effect within PBL directly inhibits the daytime PBL development. PBL suppression effect is then amplified by entrainment processes resulting in excessively low PBL height, especially for dust particles below but near the PBL top. Dust plumes weaken updrafts from PBL and downdrafts of the free atmosphere, which further reduce the entrainment mixing through attenuating horizontal and vertical advection, and eventually amplify PBL suppression. At night, near-surface dust aerosols stimulate a warm and unstable lower atmosphere, generate warm advection heating and promote the PBL development. Our study highlights the importance of specifying entrainment parameters and nighttime advection activities in quantifying the dust-PBL interactions.

1. Introduction

Mineral dust contributes to more than half of the global aerosol loading (Knippertz and Todd, 2012; Choobari et al., 2014; Guan et al., 2019). High concentration of dust aerosols generates negative socio-economic effects because they increase traffic accident rates, agriculture degradation and health risks (Merrifield et al., 2013; Aili and Oanh, 2015; Middleton et al., 2019). East Asia is one of the largest regions of dust source worldwide as a result of massive dust emission from Taklimakan Deserts in Tarim Basin (TB) (Chen et al., 2017a; Maki et al., 2019). Strong dust outbreaks in the Taklimakan Deserts occur with the highest frequency in spring, and can persist for several days to weeks

(Yumimoto et al., 2009; Ge et al., 2014; Guo et al., 2017; Hu et al., 2020). Dust particles over the TB can be easily accumulated and lifted to higher than 3 km due to the near-surface convergence flows and obstruction of complex terrains, as TB is surrounded by the Tianshan Mountains, the Kunlun Mountains, the Pamir Plateau and the Tibetan Plateau (Nan and Wang, 2018; Pan et al., 2020; Zhao et al., 2020). Suspended dust particles impose pronounced perturbations in radiation balance through attenuating solar radiation and regulating infrared radiation (Fu et al., 2009; Li et al., 2020; Wang et al., 2020a; Xu et al., 2020). Especially under the influences of unique basin topography and intense surface heating, prolonged dust residence time causes extremely strong interactions with planetary boundary layer (PBL) processes

* Corresponding author at: Key Laboratory of Meteorological Disaster, Ministry of Education (KLME)/Joint International Research Laboratory of Climate and Environment Change (ILCEC)/Collaborative Innovation Center on Forecast and Evaluation of Meteorological Disasters (CIC-FEMD), and School of Atmospheric Sciences, Nanjing University of Information Science and Technology, Nanjing 210044, China.

E-mail address: haishan@nuist.edu.cn (H. Chen).

<https://doi.org/10.1016/j.atmosres.2022.106359>

Received 18 April 2022; Received in revised form 18 July 2022; Accepted 21 July 2022

Available online 25 July 2022

0169-8095/© 2022 The Author(s). Published by Elsevier B.V. This is an open access article under the CC BY-NC-ND license (<http://creativecommons.org/licenses/by-nc-nd/4.0/>).

through dust radiative effect in the TB (Liu et al., 2016; Li et al., 2019; Tan et al., 2022).

Inherent impacts of dust radiative forcing on PBL evolution has led to a shallower daytime PBL and considerably exacerbated air pollution in the TB region and along the transport pathways of the East Asian Continent, the Pacific Ocean and even the Greenland (Bory et al., 2003; Liu et al., 2019a; Yumimoto et al., 2019). Turbulent motion in the daytime is suppressed because of dust scattering and absorbing effects on solar radiation, which increases the stratification stability and inhibits PBL development (McGrath-Spangler et al., 2015; Huang et al., 2018, 2020; Wang et al., 2021). While deficient energy input plays a key role in PBL suppression, it is by no means the sole mechanism depicting dust-PBL interactions, which are affected by various dynamic processes. Moreover, dust aerosols are reported to pose longwave radiative forcing reaching up to $30\text{--}40\text{ W}\cdot\text{m}^{-2}$ for East Asian source region (Alam et al., 2014; Han et al., 2015). However, the feedbacks between dust-induced longwave radiation effect and PBL development, especially for nocturnal PBL, are still unknown. It brings knowledge gaps in estimating impacts of dust radiative forcing on meteorological parameters and air quality at hourly and diurnal scales (Zhang et al., 2010; Sawyer and Li, 2013; Miao et al., 2017).

The dependency of the magnitude of dust radiative forcing on its vertical distributions and optical properties is under debate (Huang et al., 2009; Ge et al., 2010; Zhao et al., 2010; Liu et al., 2011). It is usually agreed that dust aerosols exert cooling effect on the underlying surface in the daytime because of less downward shortwave radiation (Haywood et al., 2003; Satheesh et al., 2007; McFarlane et al., 2009). However, the signs of dust-induced radiative effect can be reversed at the top of atmosphere (TOA), which also modulates the intensity of radiative budget and PBL processes (Pérez et al., 2006; Jish Prakash et al., 2015; Kong et al., 2022). The contrary TOA radiative forcing values depend on distinct dust vertical heights, dust-layer depths, and optical parameters (Wang et al., 2010; Zhao et al., 2011; Xin et al., 2016). Dust aerosols lofted to higher elevations over the Asian region are identified to be more absorptive than those in Africa (Costa et al., 2006; Ge et al., 2010). The relatively high absorbing efficiency of solar radiation by dust aerosols is found to reshape the atmospheric thermal structure and further complicate the interactions between dynamic fields, including monsoon circulation, heat waves, deep convection among others (Lau et al., 2006; Min et al., 2009; Cowan et al., 2020). Observational evidence also shows that vertical distribution of absorbing aerosols, e.g., dust aerosols, can regulate radiation transfer discriminatively and result in spatially varying PBL characteristics (Johnson et al., 2008; Bravo-Aranda et al., 2015; Bucci et al., 2018). Given the tremendous dust emissions in Taklimakan Deserts and the broader impacts on regional climate and socioeconomic systems, further analysis is needed to identify the spatial and temporal variability of dust radiative perturbations and its impacts on PBL evolution.

Unlike considerable attention paid to anthropogenic emissions of black carbon aerosols and their substantial impacts on PBL meteorology and climate change at regional and global scales (Redemann et al., 2021; Doherty et al., 2022), dust aerosols as another major fraction of absorbing aerosols have not been explored sufficiently in the radiative impacts on PBL structure (Xie et al., 2018; Marsden et al., 2019). In particular, the radiative effect of dust aerosols involving various vertical distributions and high absorbing efficiency on the boundary layer dynamics warrants further investigation over TB. Here, we employ the Weather Research and Forecasting model with Chemistry module (WRF-Chem) to conduct multiple experiments of a typical dust storm event in Taklimakan Desert over TB and to investigate how dust radiative effect regulates PBL processes. The objectives of this study are to (1) evaluate the impacts of dust aerosols on daytime and nighttime radiative budgets and PBL development, (2) identify the decisive factors in the daytime and nighttime dust-PBL interactions, and (3) explore the physical mechanism of dust radiative effect on PBL evolution and its implications for air pollution control.

2. Data and methods

2.1. Observation-based dust storm case

Cold frontal systems and strong surface wind are two dominant drivers for the formation of severe dust events in Eastern Asia (Jia et al., 2015; Ge et al., 2016; Wang et al., 2020b). We selected a springtime dust storm episode from April 27 to May 1, 2015 over Tarim Basin for this study. During this dust storm episode, large-scale upper-level deep troughs (500 hPa) associated with surface active cold front swept northeastwards from the Ural Mountains to TB. Subsequently, cold air from the western Siberian intruded obliquely and persisted over Tarim Basin. Due to the large air pressure gradient built by the cold front, vigorous near-surface wind blew at the junction of high and low pressure systems. Dust aerosols, which were triggered by the integrated effects of low-pressure systems and intensified flows, invaded the Tarim Basin and suspended in the atmosphere for days (Meng et al., 2019).

In this dust storm event, meteorological fields and dust aerosol distribution were measured at five observational stations located in the center and four lateral sides of TB, i.e., Kashi (KSH), Akesu (AKS), Kuerle (KEL), Tazhong (TZH) and Hetian (HT) stations (Fig. 1b). While hourly ground-level air temperature, wind speed and wind direction data were recorded at all five sites, hourly PM_{10} concentrations were obtained only at TZH and KSH stations. Vertical profiles of potential temperature and wind speed were observed at all sites, except the TZH station, by CFL-03 wind profiler radar from the radar wind profiler network of China (Liu et al., 2020).

2.2. Model configuration and experiment design

We applied WRF-Chem (version 3.9.1.1) to simulate this dust storm event. Three two-way nested domains were employed with horizontal resolution of 36, 12, and 4 km and corresponding grid cells of 200×200 , 199×229 , and 367×187 , respectively (Fig. 1a). The outermost domain (D01) spanned over Eastern Asia, while TB was in the innermost domain (D03) surrounded by the Tianshan Mountains, the Pamir Plateau and the Tibetan Plateau. The detailed topography of intermediate domain (D02) and D03 was shown in Fig. 1b. There were 76 vertical layers with terrain-following coordinates from surface to 100-hPa level. Approximately 36–42 layers stretched within 3000 m to better resolve the PBL vertical structure.

The fifth generation of European Centre for Medium-Range Weather Forecasts (ECMWF) Reanalysis data (ERA5) (Hersbach et al., 2020) provided the initial conditions and lateral boundary conditions of meteorological variables at a horizontal resolution of $0.25^\circ \times 0.25^\circ$ and an interval of 6 h. The physical and chemical parameterization schemes used in our domains were summarized in Table 1. All of the domains were specified with the Morrison double-moment microphysics scheme (Morrison et al., 2009) and the Kain-Fritsch cumulus parameterization scheme (Kain, 2004). Goddard Chemistry Aerosol Radiation and Transport (GOCART) mechanism was chosen for the aerosol and chemistry module (Chin et al., 2002). GOCART dust emission scheme embedded in WRF-Chem was also selected to calculate dust emission flux based on dust erodibility fraction, surface wind speed and threshold wind speed. The emitted dust aerosols were assumed to be spherical and divided into eight discrete size bins (0.1–0.18 μm , 0.18–0.3 μm , 0.3–0.6 μm , 0.6–1.0 μm , 1–1.8 μm , 1.8–3 μm , 3–6 μm , and 6–10 μm in particle radius) (Ginoux et al., 2001, 2004).

Radiation transfer procedure was simulated using Rapid Radiative Transfer Model for General Circulation Models (RRTMG) shortwave and longwave radiation schemes (Iacono et al., 2000, 2003, 2008). The refractive index of mineral dust for shortwave radiation was defined as $1.55 + 0.006i$ based on field observations of East Asian dust (Fukushima et al., 2000; Stone et al., 2007; Logan et al., 2013). In the longwave radiation, the refractive index of dust aerosols was strongly dependent on wavelength, and the values were adopted for 16 longwave spectral

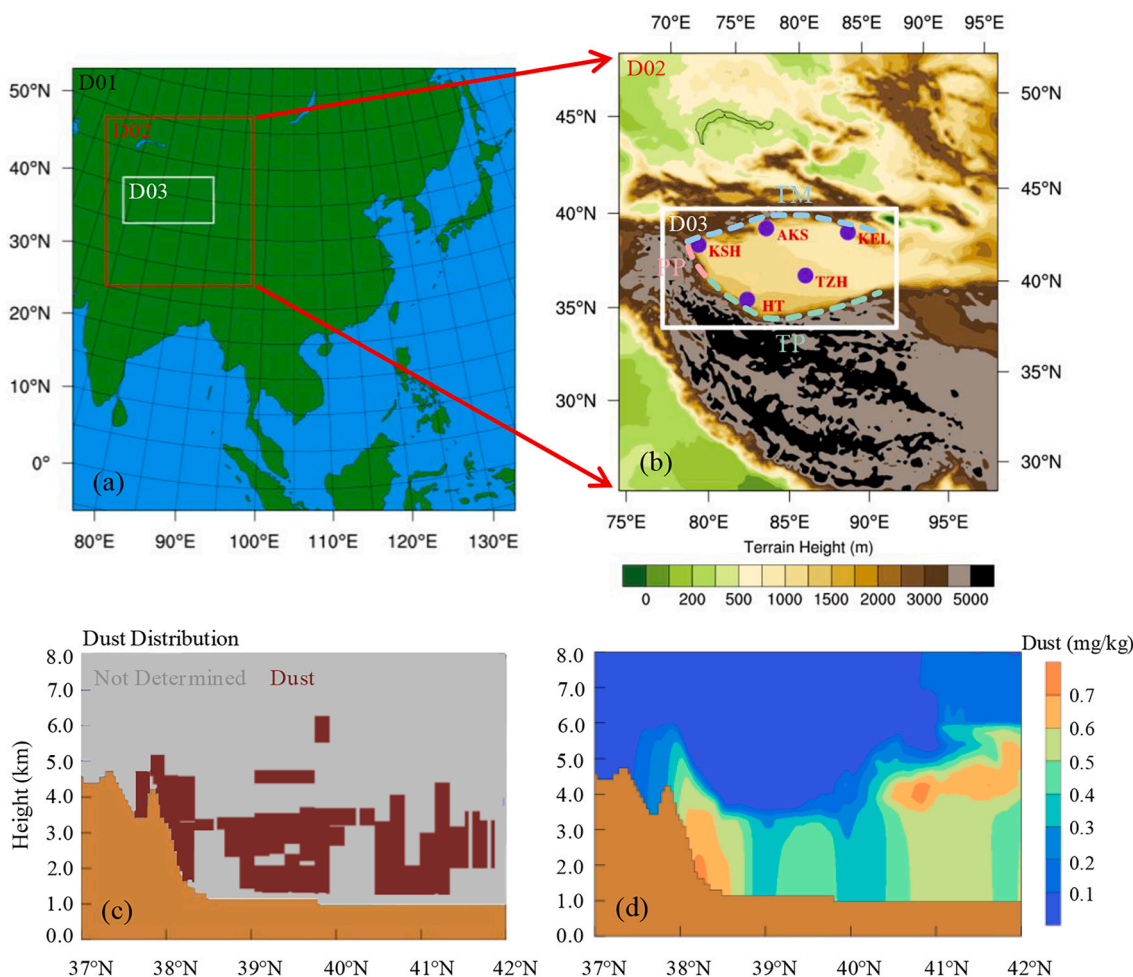


Fig. 1. The WRF-Chem Model domain of three nested meshes with horizontal resolution of 36, 12 and 4 km marked with black (D01), red (D02) and white (D03) rectangles (a), elevations of the intermediate (D02) and innermost (D03) domains with locations of five observation sites (AKS, TZH, KEL, HT and KSH) in purple dots over the Tarim Basin (b), cross-section of satellite-retrieved dust distribution at 15:30 LST (c) and simulated dust concentration distribution at 16:00 LST along the orbit path of CALIPSO on April 30, 2015 (d). The outermost domain (D01, Fig. 1a) spans over Eastern Asia and the Tarim Basin is in the innermost domain (D03, Fig. 1b) surrounded by the Tianshan Mountains (TM in the north), the Pamir Plateau (PP in the west) and the Tibetan Plateau (TP in the south). The terrain height is marked with brown colour in Figs. 1c-1d. (For interpretation of the references to colour in this figure legend, the reader is referred to the web version of this article.)

Table 1
Configuration of the WRF-Chem simulation.

Model Configurations			
Domains	D01	D02	D03
Resolution (km)	36	12	4
No. of grid points (lon × lat)	200 × 200	199 × 229	367 × 187
Vertical layers	76	76	76
Cumulus parameterization	Kain-Fritsch		
Microphysics	Morrison double-moment scheme		
Planetary boundary layer	YSU		
Shortwave radiation	RRTMG		
Longwave radiation	RRTMG		
Dust emission	GOCART		

bands according to the Optical Properties of Aerosols and Clouds dataset (Hess et al., 1998; Zhao et al., 2010; Li et al., 2021). The boundary layer evolution was simulated with the Yonsei University (YSU) PBL scheme (Hong et al., 2006). YSU scheme with non-local mixing treatment was identified to generate the best agreements with both WRF-Large Eddy Simulation (WRF-LES) model (Wang et al., 2016) and lidar and balloon observations (Hu et al., 2013) when daytime PBL development is strongly dependent on entrainment process expression. YSU has in recent years become one of most widely-used PBL schemes (e.g., Miao

et al., 2015; Sun et al., 2016; Zhu et al., 2018; Yang et al., 2019; Hu et al., 2019). Reflected with higher mean correlation coefficients (Cr), lower mean bias (MB), and lower root-mean-square errors (RMSE), the simulation results with combination of the RRTMG radiation transfer schemes and YSU PBL scheme agreed with all observations better than that simulated with the other five scheme combinations (Tables S1-S3). In particular, the RRTMG and YSU scheme combination better reproduced PM_{10} concentration and profiles of potential temperature and wind speed (Tables S2-S3).

We conducted two parallel experiments of the same model configurations and parameterization schemes, except that the aerosol radiative forcing (ARF) was turned on in the control run (Ctl) and turned off in the No-ARF run (No-ARF), to evaluate the dust radiative effects on daytime and nighttime PBL development. Each simulation run from 08:00 local standard time (LST, 8 h ahead of coordinated universal time) on April 24 to 20:00 LST on May 1, 2015, leaving the first 48 h as model spin-up period. Rather high peak values of dust emission fluxes and dust loading were detected from the daytime on April 28 to the early-morning on April 29. We then analyzed the PBL evolution on April 28 and April 29 when dust-PBL interactions were the strongest.

2.3. Simulation evaluation and improvement

To evaluate model performance in reproducing this dust storm event, we compared hourly meteorological observation data, PM_{10} concentration and vertical profiles from our Ctl experiment with the observations and simulations by Meng et al. (2019). In addition to designing finer domains and higher vertical resolution in our experiments than that in Meng's settings, we chose RRTMG shortwave and longwave schemes and YSU PBL scheme to better resolve the impacts of dust radiative effect on PBL processes. Our results improved simulations of meteorological and aerosol fields compared with Meng's results, in which 2-m air temperature was underestimated, and 10-m wind speed and PM_{10} concentration were substantially overestimated (Figs. S1-S2). These three variables have interior relationships in the circulation system. Low wind speed restricts wind-forced movement of soil dust particles, and eventually results in less suspending dust aerosols. Reduced PM_{10} concentration is responsible for higher near-surface temperature by more surface heat flux due to weakened dust light attenuation. Moreover, the reproducibility of wind speed was still challenging in both Meng's and our simulations. Although our results were better in capturing meteorological elements and particle concentration, some biases still existed, because our experiment design, even with finer spatial and vertical grid spacing, can not fully eliminate the limitation in the representation of topographic effects (Meng et al., 2019).

Potential temperature and wind speed profiles are critical to characterize the PBL structure and dust aerosol distribution pattern. Further inspection of vertical profiles showed that the time series and magnitude of potential temperature and wind speed better agreed with the radar data than that in Meng et al. (2019) (Fig. S2). A summary of performance statistics was given in Tables S4-S5 to demonstrate the improvements in our simulation. Higher correlation coefficients (Cr), lower mean bias (MB), and lower root-mean-square errors (RMSE)

values indicated that our simulation output was better in reproducing temporal and spatial variations of synoptic conditions and pollution concentration. These improvements enabled our experiment results to be reasonably used to investigate the dust-PBL interactions.

The Cloud-Aerosol Lidar and Infrared Pathfinder Satellite Observation (CALIPSO) level 2 cloud and aerosol discrimination data products provide the vertical structure of aerosol subtypes at regional and global scales (Winker et al., 2006; Huang et al., 2009). CALIPSO overpassed TB from 15:32 to 15:34 LST on April 30. We compared the cross-sectional distribution of simulated dust concentration at 16:00 LST with CALIPSO aerosol typing along the overpass section (Figs. 1c-1d). In general, the CALIPSO retrieved dust plumes extending up to about 6 km above sea level were reproduced by our numerical simulation.

Dust radiative effect in this study is quantified within each physical scheme/process including the Planetary Boundary Layer (PBL), Radiative (Ra), Advection (Ad) and Cumulus (Cu) heating rates. PBL heating rate is calculated as vertical gradients of sensible heat flux in the YSU PBL scheme, and Ra heating rate from RRTMG radiation schemes includes the contribution of shortwave and longwave fluxes. The Ad heating rate consists of both horizontal and vertical advection terms in the scalar advection module. Cu heating rate is extracted from cumulus schemes and remains zero during this dust storm event without cumulus effect.

3. Results and discussion

3.1. Opposite effects of dust on day-night boundary layer development

During the dust event, two high-value centers of dust loading were located in the east and middle of TB in the daytime, and dust plumes were accumulated with higher concentrations in a wider area of the southeast margin (Fig. 2a). Dust aerosols lowered the daytime surface

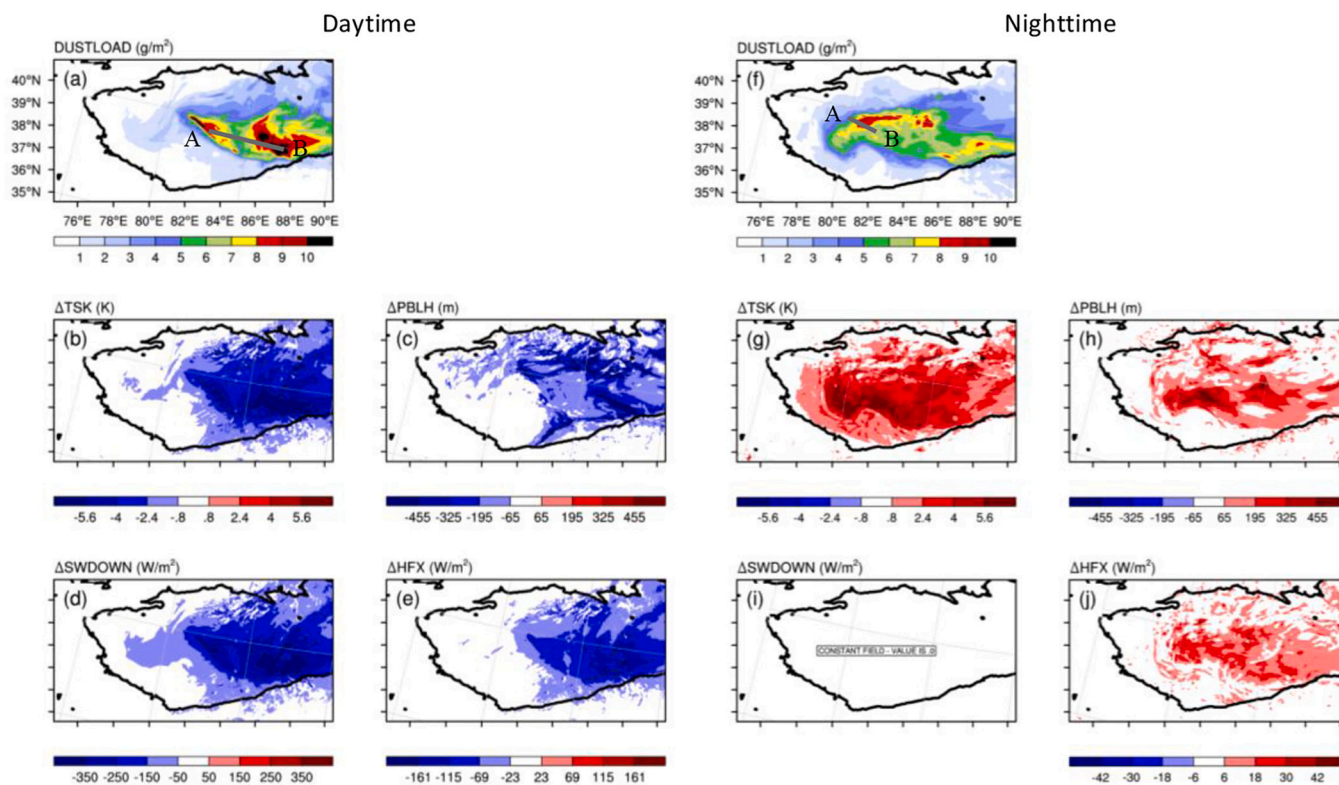


Fig. 2. Daytime and nighttime dust column loading (a, f) and differences of surface temperature (b, g), PBL height (c, h), surface downward shortwave flux (d, i) and surface heat flux (e, j) between Ctl and No-ARF experiments. Black solid lines outline the border of Tarim Basin. Fig. 2i is blank due to absence of solar radiation at night. The lines AB in (a) and (f) were used as transects to exhibit the spatial heterogeneity of dust impacts on PBL structure and to identify its decisive factors shown in Fig. 4, Fig. 5 and Fig. S5. The colorbar scales in Fig. 2e and Fig. 2j are different.

temperature and suppressed the PBL development. The TB-averaged surface temperature and PBL height reduced by 2.52 K and 164.36 m, respectively (Figs. 2b-2c). Decreases in surface temperature and PBL height were attributable to diminished shortwave flux reaching the ground and reduced surface heat flux because dust particles impeded incident solar radiation through scattering and absorbing effects (Figs. 2d-2e and Fig. 3a), and concurrently trapped more shortwave radiation in the atmosphere (Fig. 3b). The TB-averaged solar radiative forcing values were $-50.82 \text{ W}\cdot\text{m}^{-2}$ at 14:00 LST in Fig. 3 ($-37.35 \text{ W}\cdot\text{m}^{-2}$ during the daytime period from 09:00 to 20:00 LST in Fig. S3) at the surface, and $58.44 \text{ W}\cdot\text{m}^{-2}$ ($38.90 \text{ W}\cdot\text{m}^{-2}$) in the atmosphere, which were comparable to observations near Taklimakan Desert or in the downstream of TB (Ge et al., 2010; Xin et al., 2016). The magnitudes of atmospheric radiative effect caused by dust aerosols in our study were greater than the estimate of $38.79 \text{ W}\cdot\text{m}^{-2}$ over Dehradun (Patel and Kumar, 2015) and the range of $28\text{--}45 \text{ W}\cdot\text{m}^{-2}$ over the Mediterranean basin (Gkikas et al., 2018; Kaskaoutis et al., 2019), implying more absorbing dust aerosols in the northwestern China (Costa et al., 2006; Wang et al., 2009). Conversely, dust aerosols emitted more downward infrared radiation due to effective absorption of solar radiation, regulating a surplus in surface longwave radiation (Fig. 3c) and a deficit in the atmospheric longwave radiative forcing (Fig. 3d). The surface infrared radiative forcing modulated by dust aerosols in this dust storm was about $17.90 \text{ W}\cdot\text{m}^{-2}$ ($15.77 \text{ W}\cdot\text{m}^{-2}$), which is similar to simulated values in Gobi deserts (Liu et al., 2016), but greater than $14.4 \text{ W}\cdot\text{m}^{-2}$ in Central Mediterranean (Meloni et al., 2015) and $10 \text{ W}\cdot\text{m}^{-2}$ over Sal Island (Hansell et al., 2010) as a consequence of lower dust concentrations. The daytime perturbations of shortwave radiation were approximately 2–3 times that of longwave radiation. It is noteworthy that the prominent reduction region of surface temperature almost coincided with the distribution of high-level dust loading and large dust radiative forcing, while the strongest PBL suppression occurred in the eastern open mouth of TB.

At night, dust aerosols advanced westward and formed a high-concentration zone in the middle of the basin, whereas dust plumes in

the eastern center were weakened (Fig. 2f). On the contrary to the daytime, dust plumes increased surface heat flux in the nighttime, which led to a warmer surface and enhanced PBL height growth in TB by 2.58 K and 98.88 m on average, respectively (Figs. 2g-2j). Suspended dust layers, as mainly composed of coarse particles, inevitably prohibited outgoing terrestrial radiation, which thus increased the surface longwave radiation (Fig. 3e) and resulted in negative atmospheric longwave radiative forcing (Fig. 3f). The nocturnal longwave radiative effect was $10.62 \text{ W}\cdot\text{m}^{-2}$ at 02:00 LST ($10.66 \text{ W}\cdot\text{m}^{-2}$ during the nighttime period from 21:00 to 08:00 LST in Fig. S3) at the surface. This longwave radiative forcing was smaller than the values of $14\text{--}17 \text{ W}\cdot\text{m}^{-2}$ during severe Saharan dust storms of very high aerosol optical depths (AOD) (Heinold et al., 2008; Francis et al., 2022). In similar to the daytime, significant changes in nighttime PBL height were not entirely coincident with the largest dust loading and radiation flux changes.

As a result, dust-induced shortwave radiation variations prevailed in the daytime, while longwave radiation adjustments due to dust aerosols dominated at night. Such inverse surface and atmospheric radiative forcing reallocation gave rise to alternating variations in surface heat flux, and thereby opposite daytime and nighttime changes in surface temperature and PBL development in response to dust aerosol accumulation and distribution (Figs. 2-3 and S3-S4). The contrast effects of dust aerosols on diurnal and nocturnal radiation fluxes are responsible for differentiated responses of surface wind speeds, temperature gradients and the subsequent dust emissions. Weakened surface wind forces less dust production over both source and downwind regions in the daytime, while nocturnal dust emission is strengthened by stronger wind speeds. Besides, such tendencies can be reversed at the edge of plumes in the same dust event due to temperature gradients through thermal wind effect (Rémy et al., 2015; Liu et al., 2016; Chen et al., 2017b). However, these conclusions are limited to describing average changes of dust radiative effects on meteorological variables. Little attention is paid to the characteristics and mechanisms of spatial heterogeneity in dust-related radiation effects and its interactions with PBL height variations.

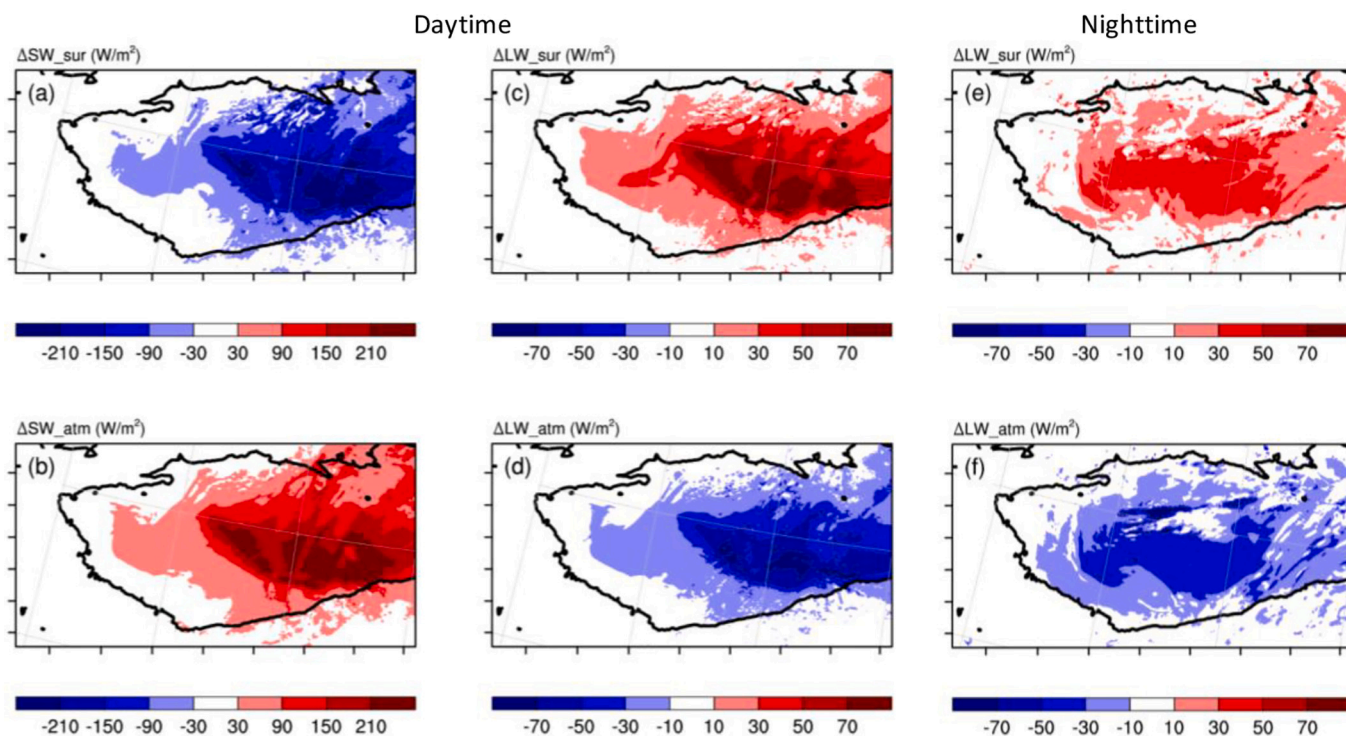


Fig. 3. Differences of daytime and nighttime shortwave (a-b) and longwave (c-d, e-f) radiative forcing at the surface (the upper panel) and in the atmosphere (the lower panel) between Ctl and No-ARF experiments. Black solid lines outline the border of Tarim Basin.

3.2. Amplified dust-PBL interactions by dust vertical distribution

The impacts of dust radiative effect on PBL development are sensitive to dust characteristics (e.g., total loading, vertical distribution and optical properties) and surface properties, such as surface albedo and soil moisture (Liu et al., 2011; Saleeby et al., 2019; Darvishi Boloorani et al., 2021). Since TB is covered by deserts with almost uniform surface albedo and low soil moisture, cross-sectional distributions of dust concentration and characteristics along the A-B lines for daytime (Fig. 2a) and nighttime (Fig. 2f) were depicted to exhibit the spatial heterogeneity of dust impacts on PBL structure and to identify its decisive factors (Fig. 4). Dust aerosols were dispersed throughout the PBL and established a well-mixed vertical distribution in the daytime with the exception of dust particles in a region transported into the higher altitudes (at around 86.7–87.6°E in Fig. 4a). Two kinds of distinct characteristics has been shown in the series of dust loading and PBL height variations (Fig. 4b). In the transect from 82.5°E to 85.8°E, PBL development showed a negative response to total dust concentration. Similar dust loading in the transects of 85.8–86.7°E and 86.7–87.6°E also triggered the suppression effect on PBL development, but with excessively low PBL height at around 86.7–87.6°E. In general, heavy dust-laden air was accompanied by more depressed daytime PBL height. However, total dust concentration was unlikely a major driving force behind the drastic encumbrance of PBL development. Moreover, optical properties are not likely to induce the excessively low PBL height at around 86.7–87.6°E because variations of the Single Scattering Albedo (SSA) and Asymmetry Factor (ASY) were small during this dust storm (Fig. 4e and f). Hence, intense light attenuation of aerosols at high altitudes (below but close to the PBL top) presumably resulted in a turning point of the abruptly strengthened dust-PBL interactions at around 86.7°E (Fig. 4a and c). This amplification effect on PBL suppression was also detected in other studies when aerosols were located near the PBL top. For example, based on 1939 samples from micropulse lidar measurements around noontime in Beijing, the shallowest PBL with the weakest

buoyancy were observed when the peak value of aerosol extinction coefficient was distributed right below the PBL top (Su et al., 2020). When aerosols were located at the PBL top, both turbulent kinetic energy and PBL height decreased steeply according to numerical simulations (Barbaro et al., 2013; Zhang et al., 2022). However, these observations or simulations from sparse stations were unable to explain the dynamic mechanism of amplification effect on PBL inhibition explicitly.

During the nighttime, variation of the total dust loading along the transect was relatively low (6.5–8 g·m⁻²). Unlike daytime, nocturnal dust aerosols were accumulated near the surface, and their concentration decreased with height because of stable atmospheric stratification (Figs. 4g–4h). It is noteworthy that dust loading and optical properties had no direct link to the pronounced PBL promotion along the transect (Fig. 4h, k and l). However, aerosols near the surface could prominently promote the nighttime boundary layer growth. When dust concentration increased in the near-surface layer, the boundary layer also became deeper (the transect of 80.8–81.5°E in Figs. 4g–4h), and vice versa. Therefore, aerosol vertical distribution tended to dramatically amplify the interactions between dust radiative effect and PBL evolution in both daytime and nighttime.

Our results highlight the importance of dust vertical distribution on the daytime and nighttime PBL development. Since aerosol datasets from routine monitoring stations and intensive field campaigns are mostly based on near-surface measurements, light attenuation of upper-level aerosols (especially during the dust storms or severe pollution events) accounts for large underestimates in quantifying aerosol effects on daytime PBL suppression (Wang et al., 2019, 2021), but is still lacking. Moreover, nighttime measurements of meteorological variables and dust characteristics are rare, which causes a research gap of dust-PBL interactions involving observation analysis, model evaluation and policy making. More vertical profiles from ground-based networks and airborne platforms are urgently needed to accurately characterize the dust distribution and PBL structure in order to improve the understanding of dust-PBL interactions.

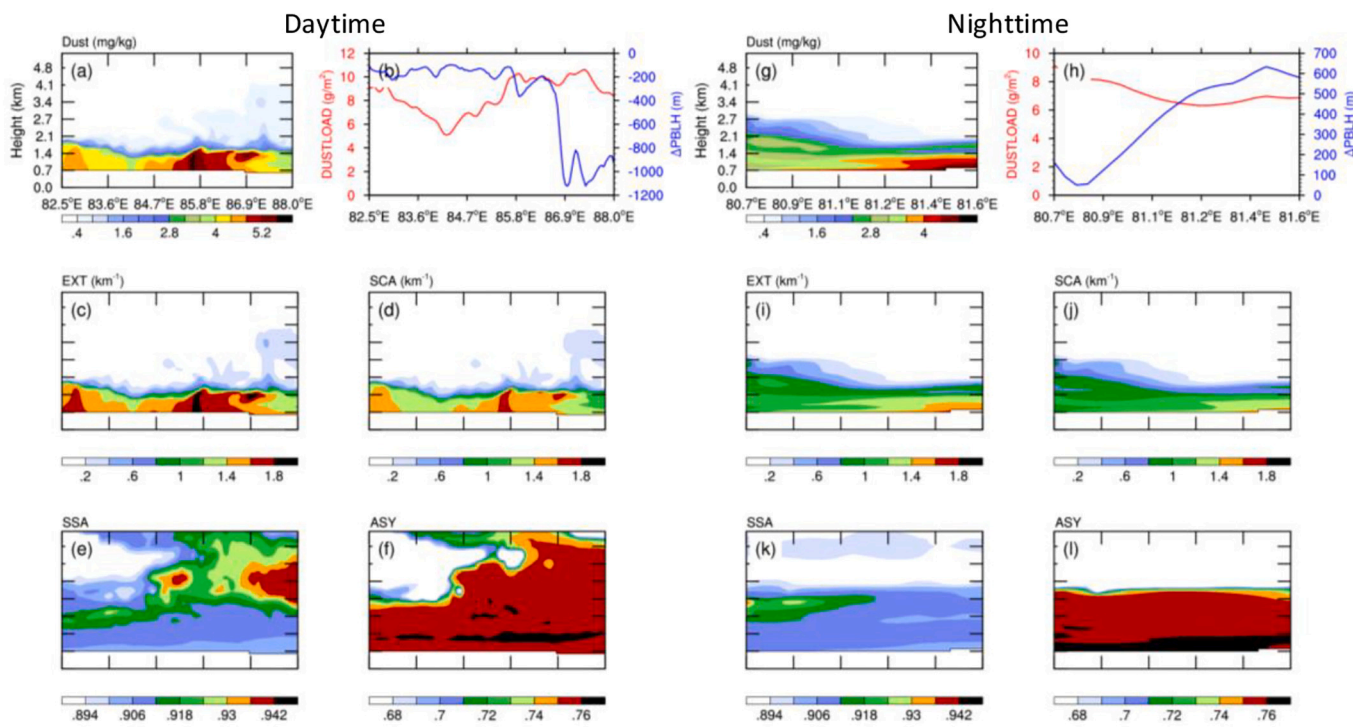


Fig. 4. Dust concentration (a, g), column dust loading (red lines in b, h), PBL height differences (blue lines in b, h) between Ctl and No-ARF experiments, extinction coefficient (c, i), scattering albedo (d, j), single scattering albedo (e, k) and asymmetry factor (f, l) in the daytime and nighttime along the AB cross-sections. The cross-sections from A to B are depicted in Fig. 2a and f for daytime and nighttime, respectively. (For interpretation of the references to colour in this figure legend, the reader is referred to the web version of this article.)

3.3. Mechanisms of dust-driven opposite day-night boundary layer development

Heating rates calculated as convergence of radiation fluxes are quantified to determine PBL processes. We discuss two types of net heating rates below, Net_{scm} and Net_{total} heating rates. Net_{scm} heating rate (sum of PBL and Ra heating rates) is usually used to diagnose the PBL evolution for idealized or sensitivity experiments ignoring advection transport. The positive and negative Net_{scm} heating rates represent the warming and cooling effect of PBL and Ra heating on PBL development, respectively. However, Net_{total} heating rate takes Ad heating rate into account and thus infers PBL dynamics in more realistic cases. Therefore, the discrepancies between Net_{scm} and Net_{total} heating rates can be attributed to the modulation effect of total advection term (sum of horizontal and vertical advection) on dust direct warming or cooling effects.

During the daytime, both downward shortwave radiation and surface heat flux were declined, which resulted in negative effects on PBL heating (PBL heating rate) (Figs. 5a-5b) and thus weakened turbulence motions. On the contrary to PBL heating, aerosols induced positive radiative forcing (Ra heating rate) due to absorption of solar radiation (Fig. 5c). Advection heating rate was also altered with opposite responses within and right above the PBL, with the drastic response at around 86.7–87.6°E (Fig. 5d). If advection processes were not taken into

account, the Net_{scm} heating rate was negative within PBL (Fig. 5f), indicating the direct cooling effect of dust aerosols on the boundary layer evolution. The strongest suppression of this cooling effect was detected when dust aerosols were distributed below but close to the PBL top (at around 86.7–87.6°E, Fig. 5f and h), which was consistent with results from WRF-Chem-Single Column Model (WRF-Chem-SCM) sensitivity experiments (Zhang et al., 2022). Total advection term further amplified the suppression on boundary layer development, and the strength of amplification was related to dust vertical distribution. When advection heating rate was included, a stronger suppression (larger negative Net_{total} heating rate) was shown within PBL and stronger enhancement (larger positive Net_{total} heating rate) right above the PBL top. The most significant amplification remained at around 86.7–87.6°E where dust aerosols were concentrated below but close to the PBL top (Fig. 5g).

The conceptual model of the amplification effect of dust vertical distribution on the daytime PBL suppression through total advection term is shown in Fig. 6. Solar radiation heats the surface during the day and initiates thermal convection. When thermal plumes penetrate into the overlying free troposphere, the updrafts encounter the strong inversion layer and deflect into horizontal momentum. Strong horizontal and sinking motions are thus generated at the density interface between the well-mixed turbulent layer and free atmosphere. Warm air in the capping inversion layer dips below into the PBL and is scoured off

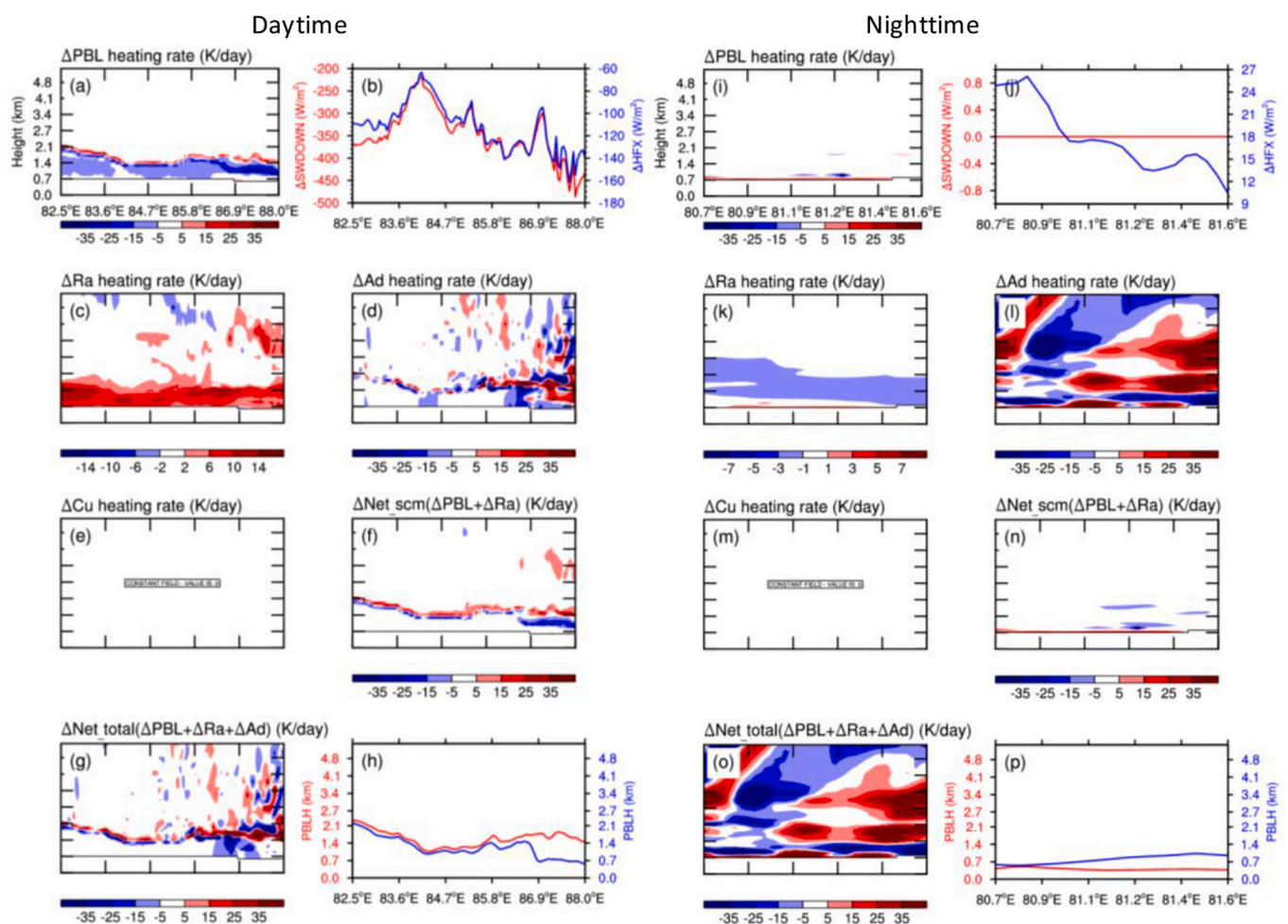


Fig. 5. Differences of PBL heating rate (a, i), surface downward shortwave flux and surface heat flux (b, j), and Radiative (c, k), Advection (d, l), Cumulus (e, m), Net_{scm} (PBL + Radiative) (f, n) and Net_{total} (PBL + Radiative+Advection) (g, o) heating rates between Ctl and No-ARF experiments in the daytime and nighttime along the AB cross-sections. PBL heights (h, p) along the AB cross-sections are from the No-ARF (red) and Ctl (blue) experiments. The cross-sections from A to B are depicted in Fig. 2a and f for daytime and nighttime, respectively. Fig. 5e and Fig. 5m are blank due to absence of cumulus effect during this dust storm episode. (For interpretation of the references to colour in this figure legend, the reader is referred to the web version of this article.)

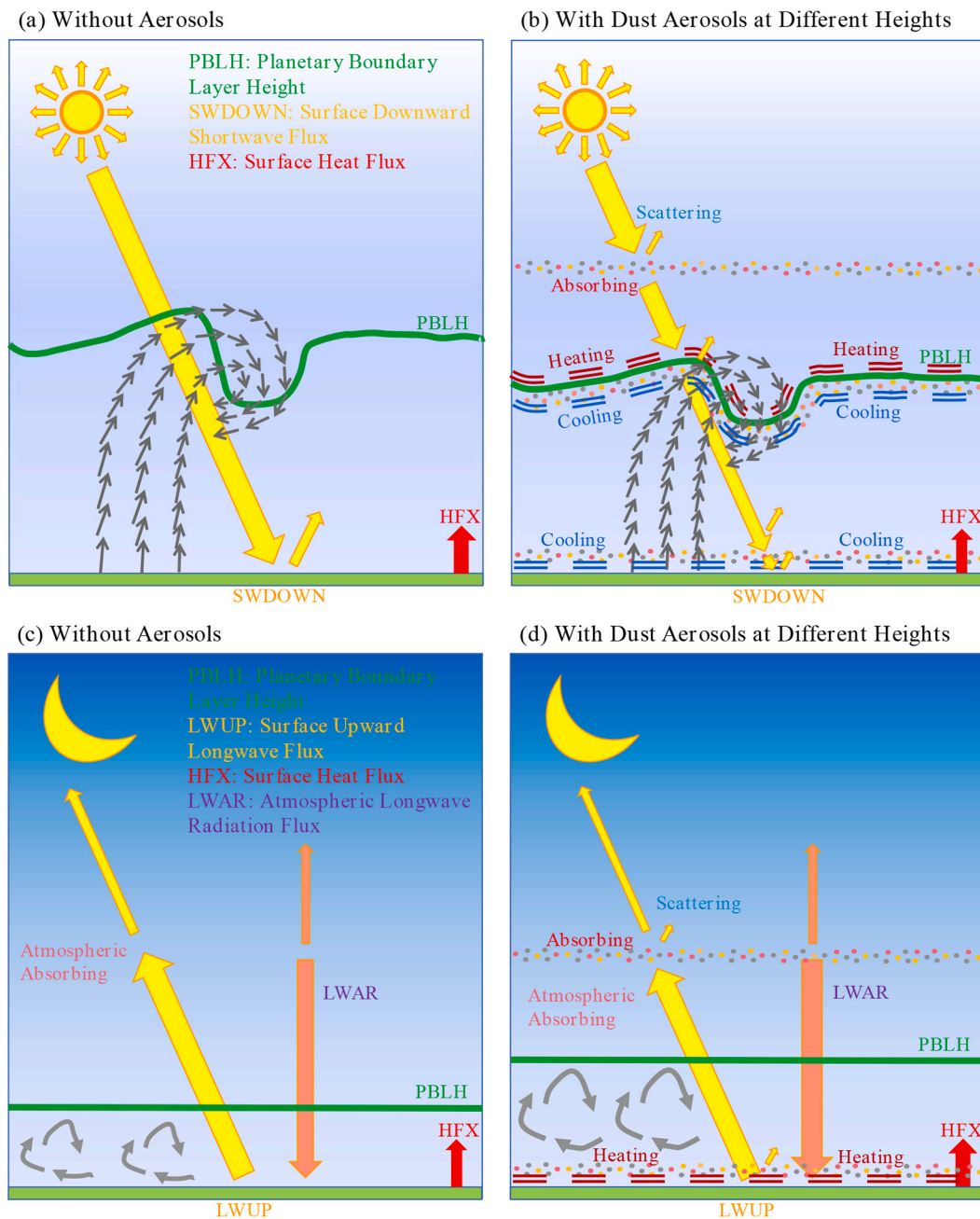


Fig. 6. Schematic illustration of interactions between entrainment, advection processes and boundary layer development without aerosols (a, c) and with dust aerosols at different heights (b, d) in the daytime (the upper panel) and nighttime (the lower panel).

by strong lateral motions. This process whereby stably stratified air from the free troposphere is mixed with the turbulent PBL is entrainment, which modifies the heat flux distribution and triggers the PBL growth (Fig. 6a) (Sullivan et al., 1998). Dust aerosols attenuate the incident solar radiation, which reduces surface heat flux, thereby causing the decline in Net_{scm} heating rate within PBL and directly inhibiting the development of the boundary layer. As the PBL top is lowered, the cooling mechanism of the original entrainment zone disappears (Hu et al., 2010). Therefore, a positive Net_{scm} heating rate dominates right above the PBL top (Zhang et al., 2022). The cooling effect within PBL and the heating effect above PBL enhance resistance in both upwelling from PBL and downwelling from the free atmosphere. This resistance further weakens entrainment processes through decreasing horizontal and vertical advection and magnifies the vertical contrast of Net_{total} heating rate, which ultimately enhances the suppression effect on PBL

development (Fig. 6b). Hence, dust aerosols exert the direct cooling effect with a negative Net_{scm} heating rate and amplification effect with entrainment mechanism on the PBL suppression. Meanwhile, the strength of this amplification effect is related to aerosol vertical distribution. Dust aerosols distributed right below the PBL top cause the weakest entrainment mixing with warm and dry air from the free troposphere and energize the strongest amplification effect on PBL suppression.

In the absence of solar radiation and insignificant PBL heating rate at night (Figs. 5i-5j), both Ra and Net_{scm} heating rates imposed very weak warming effect near the surface and cooling effect above PBL (Fig. 5k and n), showing that dust aerosols blocked outgoing longwave radiation from the surface and caused atmospheric longwave radiation deficit simultaneously. Changes in Net_{total} heating rate were determined by advection heating rate (Fig. 5l and o), especially the enhancement of

advection heating near the surface. In the nighttime, surface net radiation is regulated by upward longwave flux from the ground and atmospheric counter radiation (Fig. 6c). Dust aerosols intercept outgoing longwave radiation and reheat the surface, which leads to a warmer and more unstable near-surface atmospheric layer, and increases the low-level wind speed accordingly (Fig. S5). The combined effect of higher temperature and wind speed enhances the advection heating (Yue et al., 2010; Rémy et al., 2015), resulting in stronger nocturnal intermittent turbulence near the surface that promotes the development of boundary layer (Fig. 6d). Therefore, advection processes related to dust vertical distribution can also facilitate the impacts of dust radiative effect on nocturnal PBL evolution. The most remarkable amplification region occurs where dust aerosols are accumulated near the surface.

Our study reveals the amplification effect of entrainment and advection processes associated with dust vertical distribution on the dust-PBL interactions. If the total advection term is ignored in the daytime, aerosol-PBL interactions result in PBL suppression together with a deeper but less stable entrainment zone, which has been described in several idealized experiments of aerosol radiative effect (Barbaro et al., 2013; Liu et al., 2019b; Zhang et al., 2022). The paradox is that PBL heights are supposed to increase in response to this weakening of inversion-layer jump. As mentioned above, the single-point analysis of the aerosol shortwave radiative effect on turbulence statistics cannot reflect the complete dynamic mechanism. Our results complement this explanation and demonstrate that the advection heating rate further weakens the mixing between the PBL and free atmosphere, regardless of the stability in the entrainment zone.

For atmospheric models, basic entrainment parameters, e.g., entrainment rate and entrainment flux ratios, are usually integrated as linear relationship with surface fluxes due to lack of observational data. Actually, the entrainment ratios are dependent on both stratification and surface heat flux according to LES simulations. Heat flux profiles also become more nonlinear as aerosol optical depth increases (Liu et al., 2018). Therefore, a more comprehensive understanding is required in observational and modeling studies to uncover the basic characteristics of entrainment processes, especially under divergent aerosol loading and vertical distribution conditions. Moreover, warm advection heating is proposed as an important factor conducive to nocturnal PBL promotion. In spite of a series of observational records from monitoring networks, the distribution and intensity of nighttime advection activities associated with dust-PBL interactions are poorly understood or neglected. Hence, it is also crucial to accumulate enough datasets and theories to gain insights into nocturnal characteristics and key processes.

4. Conclusions

Under the impact of unique basin topography, abundant dust aerosols from Taklimakan Desert are injected into high altitudes and persist over Tarim Basin. We conduct numerical experiments of a springtime dust event to explore dust radiative effect on PBL development and its underlying mechanisms. We find that dust aerosols cause opposite changes in surface and atmospheric radiative energy budgets for the diurnal and nocturnal periods, which are responsible for the suppression effect in the daytime and promotion effect at night on PBL development. Besides, entrainment and advection are dominant mechanisms conducive to dust-PBL interactions. During the daytime, the dust-induced cooling effect due to diminished solar radiation directly inhibits the PBL height. Meanwhile, the cooling effect within PBL and the warming effect above PBL weaken entrainment mixing through decreasing horizontal and vertical advection and further exert the amplification effect on PBL suppression. When dust aerosols are below but close to the PBL top, the strongest amplification effect is detected with the lowest PBL height. At night, when dust plumes are concentrated near surface, the warmer near-surface atmosphere with concurrently stronger wind substantially intensifies advection and Net_{total} heating rates, which eventually lead to the PBL height growth. We also demonstrate that this

spatial heterogeneity between dust loading, radiation fluxes and PBL height variations is sensitive to dust vertical distribution. Dust particles concentrated below but close to PBL height in the daytime and near-surface dust plumes during nighttime drives the most significant amplification effect on the boundary layer evolution.

Our results highlight the importance of accurate parameterization of entrainment and nocturnal advection monitoring in detecting characteristics of dust vertical distribution and estimating its radiative effect on PBL development. Meanwhile, we propose that further observational studies providing vertical structures of dust aerosols are warranted to sufficiently demonstrate the amplification effect of dust on day-night opposite PBL development via altering the advection and entrainment processes.

Data availability statement

The ERA5 reanalysis data used in this paper are provided by the European Centre for Medium-Range Weather Forecasts (ECMWF), <https://rda.ucar.edu/datasets/ds633.0>. The CALIPSO level 2 cloud and aerosol discrimination data products are archived at <https://www-calipso.larc.nasa.gov/products>. Results of simulations in this study are available on request from the corresponding author.

CRediT authorship contribution statement

Xiaoyan Zhang: Conceptualization, Methodology, Software, Formal analysis, Investigation, Data curation, Writing – original draft, Visualization. **Xiyan Xu:** Conceptualization, Validation, Investigation, Data curation, Writing – review & editing. **Haishan Chen:** Conceptualization, Investigation, Writing – review & editing, Supervision, Project administration, Funding acquisition. **Xiao-Ming Hu:** Resources, Methodology, Software, Writing – review & editing. **Lan Gao:** Investigation, Writing – review & editing.

Declaration of Competing Interest

The authors declare no conflicts of interest.

Data availability

Data will be made available on request.

Acknowledgements

This study is jointly funded by the Natural Science Foundation of China (42021004), the DOE ASR project (DE-SC0021159) and Postgraduate Research & Practice Innovation Program of Jiangsu Province (KYCX20_0908). The first author gratefully acknowledges financial support from China Scholarship Council. We are grateful to Lu Meng for providing her model results and observations.

Appendix A. Supplementary data

Supplementary data to this article can be found online at <https://doi.org/10.1016/j.atmosres.2022.106359>.

References

- Aili, A., Oanh, N.T.K., 2015. Effects of dust storm on public health in desert fringe area: case study of northeast edge of Taklimakan Desert, China. *Atmos. Pollut. Res.* 6 (5), 805–814.
- Alam, K., Trautmann, T., Blaschke, T., Subhan, F., 2014. Changes in aerosol optical properties due to dust storms in the Middle East and Southwest Asia. *Remote Sens. Environ.* 143, 216–227.
- Barbaro, E., de Arellano, J.V.G., Krol, M.C., Holslag, A.A.M., 2013. Impacts of aerosol shortwave radiation absorption on the dynamics of an idealized convective atmospheric boundary layer. *Bound.-Layer Meteorol.* 148 (1), 31–49.

- Bory, A.J.M., Biscaye, P.E., Grousset, F.E., 2003. Two distinct seasonal Asian source regions for mineral dust deposited in Greenland (NorthGRIP). *Geophys. Res. Lett.* 30 (4).
- Bravo-Aranda, J.A., Titos, G., Granados-Muñoz, M.J., Guerrero-Rascado, J.L., Navas-Guzman, F., Valenzuela, A., et al., 2015. Study of mineral dust entrainment in the planetary boundary layer by lidar depolarisation technique. *Tellus Ser. B Chem. Phys. Meteorol.* 67 (1), 26180.
- Bucci, S., Cristofanelli, P., Decesari, S., Marinoni, A., Sandrini, S., Größ, J., et al., 2018. Vertical distribution of aerosol optical properties in the Po Valley during the 2012 summer campaigns. *Atmos. Chem. Phys.* 18 (8), 5371–5389.
- Chen, S., Huang, J., Kang, L., Wang, H., Ma, X., He, Y., et al., 2017a. Emission, transport, and radiative effects of mineral dust from the Taklimakan and Gobi deserts: comparison of measurements and model results. *Atmos. Chem. Phys.* 17 (3), 2401–2421.
- Chen, L., Zhang, M., Zhu, J., Skorokhod, A., 2017b. Model analysis of soil dust impacts on the boundary layer meteorology and air quality over East Asia in April 2015. *Atmos. Res.* 187, 42–56.
- Chin, M., Ginoux, P., Kinne, S., Torres, O., Holben, B.N., Duncan, B.N., et al., 2002. Tropospheric aerosol optical thickness from the GOCART model and comparisons with satellite and Sun photometer measurements. *J. Atmos. Sci.* 59 (3), 461–483.
- Choobari, O.A., Zawar-Reza, P., Sturman, A., 2014. The global distribution of mineral dust and its impacts on the climate system: a review. *Atmos. Res.* 138, 152–165.
- Costa, M.J., Sohn, B.J., Levizzani, V., Silva, A.M., 2006. Radiative forcing of Asian dust determined from the synergized GOME and GMS satellite data—a case study. *J. Meteorol. Soc. Jpn. Ser. II* 84 (1), 85–95.
- Cowan, T., Undorf, S., Hegerl, G.C., Harrington, L.J., Otto, F.E., 2020. Present-day greenhouse gases could cause more frequent and longer Dust Bowl heatwaves. *Nat. Clim. Chang.* 10 (6), 505–510.
- Darvishi Bolorani, A., Najafi, M.S., Mirzaie, S., 2021. Role of land surface parameter change in dust emission and impacts of dust on climate in Southwest Asia. *Nat. Hazards* 109 (1), 111–132.
- Doherty, S.J., Saide, P.E., Zuidema, P., Shinozuka, Y., Ferrada, G.A., Gordon, H., et al., 2022. Modeled and observed properties related to the direct aerosol radiative effect of biomass burning aerosol over the southeastern Atlantic. *Atmos. Chem. Phys.* 22 (1), 1–46.
- Francis, D., Nelli, N., Fonseca, R., Weston, M., Flamant, C., Cherif, C., 2022. The dust load and radiative impact associated with the June 2020 historical Saharan dust storm. *Atmos. Environ.* 268, 118808.
- Fu, Q., Thorsen, T.J., Su, J., Ge, J.M., Huang, J.P., 2009. Test of Mie-based single-scattering properties of non-spherical dust aerosols in radiative flux calculations. *J. Quant. Spectrosc. Radiat. Transf.* 110 (14–16), 1640–1653.
- Fukushima, H., Toratani, M., Yamamiya, S., Mitomi, Y., 2000. Atmospheric correction algorithms for ADEOS/OCTS Ocean color data: performance comparison based on ship and buoy measurements. *Adv. Space Res.* 25 (5), 1015–1024.
- Ge, J.M., Su, J., Ackerman, T.P., Fu, Q., Huang, J.P., Shi, J.S., 2010. Dust aerosol optical properties retrieval and radiative forcing over northwestern China during the 2008 China-US joint field experiment. *J. Geophys. Res.-Atmos.* 115 (D7).
- Ge, J.M., Huang, J.P., Xu, C.P., Qi, Y.L., Liu, H.Y., 2014. Characteristics of Taklimakan dust emission and distribution: a satellite and reanalysis field perspective. *J. Geophys. Res.-Atmos.* 119 (20), 11–772.
- Ge, J.M., Liu, H., Huang, J., Fu, Q., 2016. Taklimakan Desert nocturnal low-level jet: climatology and dust activity. *Atmos. Chem. Phys.* 16 (12), 7773–7783.
- Ginoux, P., Chin, M., Tegen, I., Prospero, J.M., Holben, B., Dubovik, O., Lin, S.J., 2001. Sources and distributions of dust aerosols simulated with the GOCART model. *J. Geophys. Res.-Atmos.* 106 (D17), 20255–20273.
- Ginoux, P., Prospero, J.M., Torres, O., Chin, M., 2004. Long-term simulation of global dust distribution with the GOCART model: correlation with North Atlantic Oscillation. *Environ. Model. Softw.* 19 (2), 113–128.
- Gkikas, A., Obiso, V., Perez Garcia-Pando, C., Jorba, O., Hatzianastassiou, N., Vendrell, L., et al., 2018. Direct radiative effects during intense Mediterranean desert dust outbreaks. *Atmos. Chem. Phys.* 18 (12), 8757–8787.
- Guan, Q., Luo, H., Pan, N., Zhao, R., Yang, L., Yang, Y., Tian, J., 2019. Contribution of dust in northern China to PM10 concentrations over the Hexi corridor. *Sci. Total Environ.* 660, 947–958.
- Guo, J., Lou, M., Miao, Y., Wang, Y., Zeng, Z., Liu, H., et al., 2017. Trans-Pacific transport of dust aerosols from East Asia: insights gained from multiple observations and modeling. *Environ. Pollut.* 230, 1030–1039.
- Han, Y., Wu, Y., Wang, T., Zhuang, B., Li, S., Zhao, K., 2015. Impacts of elevated-aerosol-layer and aerosol type on the correlation of AOD and particulate matter with ground-based and satellite measurements in Nanjing, Southeast China. *Sci. Total Environ.* 532, 195–207.
- Hansell, R.A., Tsay, S.C., Ji, Q., Hsu, N.C., Jeong, M.J., Wang, S.H., et al., 2010. An assessment of the surface longwave direct radiative effect of airborne Saharan dust during the NAMMA field campaign. *J. Atmos. Sci.* 67 (4), 1048–1065.
- Haywood, J., Francis, P., Osborne, S., Glew, M., Loeb, N., Highwood, E., Hirst, E., 2003. Radiative properties and direct radiative effect of Saharan dust measured by the C-130 aircraft during SHADE. I. Solar spectrum. *J. Geophys. Res. Atmos.* 108 (D18).
- Heinold, B., Tegen, I., Schepanski, K., Hellmuth, O., 2008. Dust radiative feedback on Saharan boundary layer dynamics and dust mobilization. *Geophys. Res. Lett.* 35 (20).
- Hersbach, H., Bell, B., Berrisford, P., Hirahara, S., Horányi, A., Muñoz-Sabater, J., et al., 2020. The ERA5 global reanalysis. *Q. J. R. Meteorol. Soc.* 146, 1999–2049.
- Hess, M., Koepke, P., Schult, I., 1998. Optical properties of aerosols and clouds: the software package OPAC. *Bull. Am. Meteorol. Soc.* 79 (5), 831–844.
- Hong, S.Y., Noh, Y., Dudhia, J., 2006. A new vertical diffusion package with an explicit treatment of entrainment processes. *Mon. Weather Rev.* 134 (9), 2318–2341.
- Hu, X.M., Nielsen-Gammon, J.W., Zhang, F., 2010. Evaluation of three planetary boundary layer schemes in the WRF model. *J. Appl. Meteorol. Climatol.* 49 (9), 1831–1844.
- Hu, X.M., Klein, P.M., Xue, M., 2013. Evaluation of the updated YSU planetary boundary layer scheme within WRF for wind resource and air quality assessments. *J. Geophys. Res.-Atmos.* 118 (18), 10–490.
- Hu, X.M., Xue, M., Kong, F., Zhang, H., 2019. Meteorological conditions during an ozone episode in Dallas-Fort Worth, Texas, and impact of their modeling uncertainties on air quality prediction. *J. Geophys. Res.-Atmos.* 124 (4), 1941–1961.
- Hu, Z., Huang, J., Zhao, C., Jin, Q., Ma, Y., Yang, B., 2020. Modeling dust sources, transport, and radiative effects at different altitudes over the Tibetan Plateau. *Atmos. Chem. Phys.* 20 (3), 1507–1529.
- Huang, J., Fu, Q., Su, J., Tang, Q., Minnis, P., Hu, Y., et al., 2009. Taklimakan dust aerosol radiative heating derived from CALIPSO observations using the Fu-Liou radiation model with CERES constraints. *Atmos. Chem. Phys.* 9 (12), 4011–4021.
- Huang, X., Wang, Z., Ding, A., 2018. Impact of aerosol-PBL interaction on haze pollution: multiyear observational evidences in North China. *Geophys. Res. Lett.* 45 (16), 8596–8603.
- Huang, X., Ding, A., Wang, Z., Ding, K., Gao, J., Chai, F., Fu, C., 2020. Amplified transboundary transport of haze by aerosol-boundary layer interaction in China. *Nat. Geosci.* 13 (6), 428–434.
- Iacono, M.J., Mlawer, E.J., Clough, S.A., Morcrette, J.J., 2000. Impact of an improved longwave radiation model, RRTM, on the energy budget and thermodynamic properties of the NCAR community climate model, CCM3. *J. Geophys. Res.-Atmos.* 105 (D11), 14873–14890.
- Iacono, M.J., Delamere, J.S., Mlawer, E.J., Clough, S.A., 2003. Evaluation of upper tropospheric water vapor in the NCAR Community Climate Model (CCM3) using modeled and observed HIRS radiances. *J. Geophys. Res.-Atmos.* 108 (D2), ACL–1.
- Iacono, M.J., Delamere, J.S., Mlawer, E.J., Shephard, M.W., Clough, S.A., Collins, W.D., 2008. Radiative forcing by long-lived greenhouse gases: Calculations with the AER radiative transfer models. *J. Geophys. Res.-Atmos.* 113 (D13).
- Jia, R., Liu, Y., Chen, B., Zhang, Z., Huang, J., 2015. Source and transportation of summer dust over the Tibetan Plateau. *Atmos. Environ.* 123, 210–219.
- Jish Prakash, P., Stenchikov, G., Kalenderski, S., Osipov, S., Bangalath, H., 2015. The impact of dust storms on the Arabian Peninsula and the Red Sea. *Atmos. Chem. Phys.* 15 (1), 199–222.
- Johnson, B.T., Heese, B., McFarlane, S.A., Chazette, P., Jones, A., Bellouin, N., 2008. Vertical distribution and radiative effects of mineral dust and biomass burning aerosol over West Africa during DABEX. *J. Geophys. Res.-Atmos.* 113 (D23).
- Kain, J.S., 2004. The Kain-Fritsch convective parameterization: an update. *J. Appl. Meteorol.* 43 (1), 170–181.
- Kaskaoutis, D.G., Dumka, U.C., Rashki, A., Psiloglou, B.E., Gavril, A., Mofidi, A., et al., 2019. Analysis of intense dust storms over the eastern Mediterranean in March 2018: impact on radiative forcing and Athens air quality. *Atmos. Environ.* 209, 23–39.
- Knippertz, P., Todd, M.C., 2012. Mineral dust aerosols over the Sahara: meteorological controls on emission and transport and implications for modeling. *Rev. Geophys.* 50 (1).
- Kong, S.S.K., Pani, S.K., Griffith, S.M., Ou-Yang, C.F., Babu, S.R., Chuang, M.T., Lin, N.H., 2022. Distinct transport mechanisms of East Asian dust and the impact on downwind marine and atmospheric environments. *Sci. Total Environ.* 154255.
- Lau, K.M., Kim, M.K., Kim, K.M., 2006. Asian summer monsoon anomalies induced by aerosol direct forcing: the role of the Tibetan Plateau. *Clim. Dyn.* 26 (7), 855–864.
- Li, Z., Wang, Y., Guo, J., Zhao, C., Cribb, M.C., Dong, X., et al., 2019. East Asian study of tropospheric aerosols and their impact on regional clouds, precipitation, and climate (EAST-AIRCPC). *J. Geophys. Res.-Atmos.* 124 (23), 13026–13054.
- Li, L., Li, Z., Chang, W., Ou, Y., Goloub, P., Li, C., et al., 2020. Aerosol solar radiative forcing near the Taklimakan Desert based on radiative transfer and regional meteorological simulations during the Dust Aerosol Observation-Kashi campaign. *Atmos. Chem. Phys.* 20 (18), 10845–10864.
- Li, L., Mahowald, N.M., Miller, R.L., Pérez García-Pando, C., Klose, M., Hamilton, D.S., et al., 2021. Quantifying the range of the dust direct radiative effect due to source mineralogy uncertainty. *Atmos. Chem. Phys.* 21 (5), 3973–4005.
- Liu, Y., Huang, J., Shi, G., Takamura, T., Khatri, P., Bi, J., et al., 2011. Aerosol optical properties and radiative effect determined from sky-radiometer over Loess Plateau of Northwest China. *Atmos. Chem. Phys.* 11 (22), 11455–11463.
- Liu, L., Huang, X., Ding, A., Fu, C., 2016. Dust-induced radiative feedbacks in North China: a dust storm episode modeling study using WRF-Chem. *Atmos. Environ.* 129, 43–54.
- Liu, C., Fedorovich, E., Huang, J., 2018. Revisiting entrainment relationships for shear-free and sheared convective boundary layers through large-eddy simulations. *Q. J. R. Meteorol. Soc.* 144 (716), 2182–2195.
- Liu, L., Guo, J., Gong, H., Li, Z., Chen, W., Wu, R., et al., 2019a. Contrasting influence of Gobi and Taklimakan deserts on the dust aerosols in western North America. *Geophys. Res. Lett.* 46 (15), 9064–9071.
- Liu, C., Fedorovich, E., Huang, J., Hu, X.M., Wang, Y., Lee, X., 2019b. Impact of aerosol shortwave radiative heating on entrainment in the atmospheric convective boundary layer: a large-eddy simulation study. *J. Atmos. Sci.* 76 (3), 785–799.
- Liu, B., Guo, J., Gong, W., Shi, L., Zhang, Y., Ma, Y., 2020. Characteristics and performance of wind profiles as observed by the radar wind profiler network of China. *Atmos. Meas. Tech.* 13 (8), 4589–4600.
- Logan, T., Xi, B., Dong, X., 2013. A comparison of the mineral dust absorptive properties between two Asian dust events. *Atmosphere* 4 (1), 1–16.
- Maki, T., Bin, C., Kai, K., Kawai, K., Fujita, K., Ohara, K., et al., 2019. Vertical distributions of airborne microorganisms over Asian dust source region of Taklimakan and Gobi Desert. *Atmos. Environ.* 214, 116848.

- Marsden, N.A., Ullrich, R., Möhler, O., Eriksen Hammer, S., Kandler, K., Cui, Z., et al., 2019. Mineralogy and mixing state of north African mineral dust by online single-particle mass spectrometry. *Atmos. Chem. Phys.* 19 (4), 2259–2281.
- McFarlane, S.A., Kassianov, E.I., Barnard, J., Flynn, C., Ackerman, T.P., 2009. Surface shortwave aerosol radiative forcing during the Atmospheric Radiation Measurement Mobile Facility deployment in Niamey, Niger. *J. Geophys. Res. Atmos.* 114 (D13).
- McGrath-Spangler, E.L., Molod, A., Ott, L.E., Pawson, S., 2015. Impact of planetary boundary layer turbulence on model climate and tracer transport. *Atmos. Chem. Phys.* 15 (13), 7269–7286.
- Meloni, D., Junkermann, W., Di Sarra, A., Cacciani, M., De Silvestri, L., Di Iorio, T., et al., 2015. Altitude-resolved shortwave and longwave radiative effects of desert dust in the Mediterranean during the GAMARF campaign: indications of a net daily cooling in the dust layer. *J. Geophys. Res.-Atmos.* 120 (8), 3386–3407.
- Meng, L., Yang, X., Zhao, T., He, Q., Lu, H., Mamtimin, A., et al., 2019. Modeling study on three-dimensional distribution of dust aerosols during a dust storm over the Tarim Basin, Northwest China. *Atmos. Res.* 218, 285–295.
- Merrifield, A., Schindeler, S., Jalaludin, B., Smith, W., 2013. Health effects of the September 2009 dust storm in Sydney, Australia: did emergency department visits and hospital admissions increase? *Environ. Health* 12 (1), 1–7.
- Miao, Y., Hu, X.M., Liu, S., Qian, T., Xue, M., Zheng, Y., Wang, S., 2015. Seasonal variation of local atmospheric circulations and boundary layer structure in the Beijing-Tianjin-Hebei region and implications for air quality. *J. Adv. Model. Earth Syst.* 7 (4), 1602–1626.
- Miao, Y., Guo, J., Liu, S., Liu, H., Li, Z., Zhang, W., Zhai, P., 2017. Classification of summertime synoptic patterns in Beijing and their associations with boundary layer structure affecting aerosol pollution. *Atmos. Chem. Phys.* 17 (4), 3097–3110.
- Middleton, N., Tozer, P., Tozer, B., 2019. Sand and dust storms: underrated natural hazards. *Disasters* 43 (2), 390–409.
- Min, Q.L., Li, R., Lin, B., Joseph, E., Wang, S., Hu, Y., et al., 2009. Evidence of mineral dust altering cloud microphysics and precipitation. *Atmos. Chem. Phys.* 9 (9), 3223–3231.
- Morrison, H., Thompson, G., Tatarskii, V., 2009. Impact of cloud microphysics on the development of trailing stratiform precipitation in a simulated squall line: comparison of one-and two-moment schemes. *Mon. Weather Rev.* 137 (3), 991–1007.
- Nan, Y., Wang, Y., 2018. De-coupling interannual variations of vertical dust extinction over the Taklimakan Desert during 2007–2016 using CALIOP. *Sci. Total Environ.* 633, 608–617.
- Pan, H., Huo, W., Wang, M., Zhang, J., Meng, L., Kumar, K.R., Devi, N.L., 2020. Insight into the climatology of different sand-dust aerosol types over the Taklimakan Desert based on the observations from radiosonde and A-train satellites. *Atmos. Environ.* 238, 117705.
- Patel, P.N., Kumar, R., 2015. Estimation of aerosol characteristics and radiative forcing during dust events over Dehradun. *Aerosol Air Qual. Res.* 15 (5), 2082–2093.
- Pérez, C., Nickovic, S., Pejanovic, G., Baldasano, J.M., Özsoy, E., 2006. Interactive dust-radiation modeling: a step to improve weather forecasts. *J. Geophys. Res.-Atmos.* 111 (D16).
- Redemann, J., Wood, R., Zuidema, P., Doherty, S.J., Luna, B., LeBlanc, S.E., et al., 2021. An overview of the ORACLES (Observations of Aerosols above Clouds and their interactions) project: aerosol–cloud–radiation interactions in the Southeast Atlantic basin. *Atmos. Chem. Phys.* 21 (3), 1507–1563.
- Rémy, S., Benedetti, A., Bozzo, A., Haiden, T., Jones, L., Razinger, M., et al., 2015. Feedbacks of dust and boundary layer meteorology during a dust storm in the eastern Mediterranean. *Atmos. Chem. Phys.* 15 (22), 12909–12933.
- Saleeby, S.M., van den Heever, Bukowski, J., Walker, A.L., Solbrig, J.E., Atwood, S.A., Miller, S.D., 2019. The influence of simulated surface dust lofting and atmospheric loading on radiative forcing. *Atmos. Chem. Phys.* 19 (15), 10279–10301.
- Satheesh, S.K., Dutt, C.B.S., Srinivasan, J., Rao, U.R., 2007. Atmospheric warming due to dust absorption over Afro-Asian regions. *Geophys. Res. Lett.* 34 (4).
- Sawyer, V., Li, Z., 2013. Detection, variations and intercomparison of the planetary boundary layer depth from radiosonde, lidar and infrared spectrometer. *Atmos. Environ.* 79, 518–528.
- Stone, R.S., Anderson, G.P., Andrews, E., Dutton, E.G., Shettle, E.P., Berk, A., 2007. Incursions and radiative impact of Asian dust in northern Alaska. *Geophys. Res. Lett.* 34 (14).
- Su, T., Li, Z., Li, C., Li, J., Han, W., Shen, C., et al., 2020. The significant impact of aerosol vertical structure on lower atmosphere stability and its critical role in aerosol–planetary boundary layer (PBL) interactions. *Atmos. Chem. Phys.* 20 (6), 3713–3724.
- Sullivan, P.P., Moeng, C.H., Stevens, B., Lenschow, D.H., Mayor, S.D., 1998. Structure of the entrainment zone capping the convective atmospheric boundary layer. *J. Atmos. Sci.* 55 (19), 3042–3064.
- Sun, X., Xue, M., Brotzge, J., McPherson, R.A., Hu, X.M., Yang, X.Q., 2016. An evaluation of dynamical downscaling of Central Plains summer precipitation using a WRF-based regional climate model at a convection-permitting 4 km resolution. *J. Geophys. Res.-Atmos.* 121 (23), 13–801.
- Tan, Z., Liu, Y., Zhu, Q., Bi, J., 2022. Effect of dust aerosols on the heat exchange over the Taklimakan Desert. *Atmos. Environ.* 276, 119058.
- Wang, C., Jeong, G.R., Mahowald, N., 2009. Particulate absorption of solar radiation: anthropogenic aerosols vs. dust. *Atmos. Chem. Phys.* 9 (12), 3935–3945.
- Wang, H., Zhang, X., Gong, S., Chen, Y., Shi, G., Li, W., 2010. Radiative feedback of dust aerosols on the East Asian dust storms. *J. Geophys. Res.-Atmos.* 115 (D23).
- Wang, W., Shen, X., Huang, W., 2016. A comparison of boundary-layer characteristics simulated using different parametrization schemes. *Bound.-Layer Meteorol.* 161 (2), 375–403.
- Wang, Z., Huang, X., Ding, A., 2019. Optimization of vertical grid setting for air quality modelling in China considering the effect of aerosol-boundary layer interaction. *Atmos. Environ.* 210, 1–13.
- Wang, T., Han, Y., Huang, J., Sun, M., Jian, B., Huang, Z., Yan, H., 2020a. Climatology of dust-forced radiative heating over the Tibetan Plateau and its surroundings. *J. Geophys. Res.-Atmos.* 125 (17) e2020JD032942.
- Wang, Z., Huang, X., Wang, N., Xu, J., Ding, A., 2020b. Aerosol-radiation interactions of dust storm deteriorate particle and ozone pollution in East China. *J. Geophys. Res.-Atmos.* 125 (24) e2020JD033601.
- Wang, Z., Huang, X., Ding, K., Ren, C., Cao, L., Zhou, D., et al., 2021. Weakened aerosol-PBL interaction during COVID-19 lockdown in northern China. *Geophys. Res. Lett.* 48 (3) e2020GL090542.
- Winker, D., Vaughan, M., Hunt, W., 2006. The CALIPSO mission and initial results from CALIOP. *Proc. SPIE* 6409, 640902.
- Xie, X., Liu, X., Che, H., Xie, X., Wang, H., Li, J., et al., 2018. Modeling East Asian dust and its radiative feedbacks in CAM4-BAM. *J. Geophys. Res.-Atmos.* 123 (2), 1079–1096.
- Xin, J., Gong, C., Wang, S., Wang, Y., 2016. Aerosol direct radiative forcing in desert and semi-desert regions of northwestern China. *Atmos. Res.* 171, 56–65.
- Xu, X., Wu, H., Yang, X., Xie, L., 2020. Distribution and transport characteristics of dust aerosols over Tibetan Plateau and Taklimakan Desert in China using MERRA-2 and CALIPSO data. *Atmos. Environ.* 237, 117670.
- Yang, Y., Hu, X.M., Gao, S., Wang, Y., 2019. Sensitivity of WRF simulations with the YSU PBL scheme to the lowest model level height for a sea fog event over the Yellow Sea. *Atmos. Res.* 215, 253–267.
- Yue, X., Wang, H., Liao, H., Fan, K., 2010. Simulation of dust aerosol radiative feedback using the GMOD: 2. Dust-climate interactions. *J. Geophys. Res.-Atmos.* 115 (D4).
- Yumimoto, K., Eguchi, K., Uno, I., Takemura, T., Liu, Z., Shimizu, A., Sugimoto, N., 2009. An elevated large-scale dust veil from the Taklimakan Desert: intercontinental transport and three-dimensional structure as captured by CALIPSO and regional and global models. *Atmos. Chem. Phys.* 9 (21), 8545–8558.
- Yumimoto, K., Kajino, M., Tanaka, T.Y., Uno, I., 2019. Dust vortex in the Taklimakan Desert by himawari-8 high frequency and resolution observation. *Sci. Rep.* 9 (1), 1–7.
- Zhang, Y., Wen, X.Y., Jang, C.J., 2010. Simulating chemistry–aerosol–cloud–radiation–climate feedbacks over the continental US using the online-coupled Weather Research Forecasting Model with chemistry (WRF/Chem). *Atmos. Environ.* 44 (29), 3568–3582.
- Zhang, X., Cai, C., Hu, X.M., Gao, L., Xu, X., Hu, J., Chen, H., 2022. Aerosols consistently suppress the convective boundary layer development. *Atmos. Res.* 106032.
- Zhao, C., Liu, X., Leung, L.R., Johnson, B., McFarlane, S.A., Gustafson Jr., W.L., et al., 2010. The spatial distribution of mineral dust and its shortwave radiative forcing over North Africa: modeling sensitivities to dust emissions and aerosol size treatments. *Atmos. Chem. Phys.* 10 (18), 8821–8838.
- Zhao, C., Liu, X., Ruby Leung, L., Hagos, S., 2011. Radiative impact of mineral dust on monsoon precipitation variability over West Africa. *Atmos. Chem. Phys.* 11 (5), 1879–1893.
- Zhao, J., Ma, X., Wu, S., Sha, T., 2020. Dust emission and transport in Northwest China: WRF-Chem simulation and comparisons with multi-sensor observations. *Atmos. Res.* 241, 104978.
- Zhu, J., Kong, F., Hu, X.M., Guo, Y., Ran, L., Lei, H., 2018. Impact of soil moisture uncertainty on summertime short-range ensemble forecasts. *Adv. Atmos. Sci.* 35 (7), 839–852.